International Journal of Nanomedicine

Dovepress
open access to scientific and medical research

Open Access Full Text Article

ORIGINAL RESEARCH

Chondroitin Sulfate Targeting Nanodrug Achieves Near-Infrared Fluorescence-Guided Chemotherapy Against Triple-Negative Breast Primary and Lung Metastatic Cancer

Chen Huang[1,*], Chunbin Li[2,3,*], Jiaxuan Cai[1,4,*], Jie Chen[1], Baobei Wang[1], Mengxia Li[1], Wei Zhou[5], Jianguo Wang[3], Pengfei Zhang[2], Jian V Zhang[1]

[1]Center for Energy Metabolism and Reproduction, Shenzhen Key Laboratory of Metabolic Health, Shenzhen Institute of Advanced Technology, Chinese Academy of Sciences, Shenzhen, People's Republic of China; [2]Guangdong Key Laboratory of Nanomedicine, CAS Key Laboratory of Health Informatics, Shenzhen Bioactive Materials Engineering Laboratory for Medicine, Institute of Biomedicine and Biotechnology, Shenzhen Institute of Advanced Technology, Chinese Academy of Sciences, Shenzhen, People's Republic of China; [3]College of Chemistry and Chemical Engineering, Inner Mongolia University, Hohhot, People's Republic of China; [4]Shenzhen College of Advanced Technology, University of Chinese Academy of Sciences, Shenzhen, People's Republic of China; [5]Gynecology Department, Huazhong University of Science and Technology Union, Shenzhen Hospital, Shenzhen, Guangdong, People's Republic of China

*These authors contributed equally to this work

Correspondence: Jian V Zhang; Pengfei Zhang, Shenzhen Institute of Advance Technology, Chinese Academy of Sciences, Shenzhen, Guangdong, 518055, People's Republic of China, Tel +86 0755-86392591, Fax +86 0755-86585222, Email jian.zhang@siat.ac.cn; pf.zhang@siat.ac.cn

Introduction: Lack of highly expressed tumor target and ligands limits application of nano-medicine against triple-negative breast cancer (TNBC). Previous study reported that placenta-derived oncofetal chondroitin sulfate glycosaminoglycan chain (CSA) expressed on 90% of stage I–III invasive ductal breast carcinomas. Our study found the CSA anchor protein VAR2CSA derived small peptide plCSA had strong binding activity with TNBC cell lines and tumor tissue. Here, we combined the AIEgens TBZ-DPNA and therapy drug paclitaxel (PTX) to fabricate near-infrared fluorescence-guided nanodrug (plCSA-NP) to investigate its targeting and anti-tumor effect on TNBC.

Methods: We synthesized and purified TBZ-DPNA with one step, measured optical properties and photoluminescence (PL) spectra. We prepared nanodrug plCSA-NP by encapsulating TBZ-DPNA and PTX and conjugating them with peptide plCSA. We evaluated plCSA-NP targeting activity by examining AIEdots fluorescence signal on TNBC cell lines and subcutaneous and lung metastatic mouse model. We assessed PTX delivery effect by cytotoxicity assay on TNBC line and tumor growth of subcutaneous and lung metastatic mouse models.

Results: PL spectra and TEM imaging results showed plCSA-NP had maximum emission feature at 718 nm and nearly monodispersed nanosphere with an average diameter of 70 nm. In vitro studies showed plCSA-NPs had high affinity and cytotoxicity with TNBC cell lines. In vivo subcutaneous and lung metastasis mouse studies showed plCSA-NPs accumulated on TNBC tumor tissue, and significantly prevented TNBC subcutaneous and lung metastasis tumor growth.

Conclusion: In conclusion, we provide solid evidence for chondroitin sulfate targeting peptide plCSA guided nanodrug, exhibit good targeting efficiency and therapeutic effect against TNBC primary and lung metastatic tumor growth.

Keywords: triple-negative breast cancer, lung metastasis, chemotherapy, aggregation-induced emission, drug delivery system, plCSA

Introduction

Breast cancer (BC) is one of the most common malignancies and a leading cause of cancer-related mortality in women worldwide.[1–3] Among them, 15% to 20% of breast carcinomas are classified as triple-negative breast cancer (TNBC), due to lack of oestrogen receptors (ER), progesterone receptors (PR) and human epidermal growth factor receptor-2

Received: 13 July 2022
Accepted: 27 October 2022
Published: 22 November 2022

(HER2).[4,5] Compared with other subtypes, TNBC is associated with high recurrence rates, a high incidence of distant metastases, and poor overall survival.[6] Although chemotherapy has shown promising results in the neoadjuvant and metastatic settings, only 20% of TNBC patients present a pathologically complete response after neoadjuvant chemotherapy.[7–10] Most unsatisfactory long-term outcomes, including premature death, were due to early recurrence and metastatic disease.[11] More importantly, chemotherapeutic drugs typically display poor pharmacokinetics (being rapidly cleared from the circulation), and inappropriate biodistribution due to their low molecular weight and high hydrophobicity (causing toxicity of various healthy tissues).[12] To minimize these concerns, albumin-bound (*nab*)-paclitaxel, a typical albumin nanoparticle carrying the therapeutic drug paclitaxel (PTX), has resulted in an advantageous pharmacokinetic (PK) profile and high tumor accumulation.[13] Currently, atezolizumab, a monoclonal antibody targeting PD-L1 combined with *nab*-paclitaxel, has demonstrated better results in early-stage TNBC and metastatic TNBC.[14–18] Unfortunately, these promising results will only benefit patients in the PD-L1-positive subgroup.

It is well known that the lack of molecular biomarkers limits the application of nanomedicine. A previous report showed that placental oncofetal chondroitin sulfate glycosaminoglycan chain (CSA), a placenta-exclusively expressed CSA (pl-CS), which binds the malarial anchor protein VAR2CSA to avoid malaria-infected erythrocyte host clearance, is expressed in 90% of stage I-III invasive ductal breast carcinomas.[19–22] Recombinant VAR2CSA has strong binding activity with primary human breast cancer and metastatic BC cancer cells.[23–25] According to the structure of VSAR2CSA, the minimal CSA binding region of VAS2CSA consists of the Duffy Binding Ligand-like (DBL) 2X domain with flanking interdomain (ID) regions. Further screening was performed on this region, and a small peptide that selectively binds to CSA was identified and then synthesized as placental CSA binding peptide (plCSA-BP, here abbreviated as plCSA).[26–29] As a result, the peptide plCSA could be applied as a targeted ligand for developing an actively targeted nano-delivery system for TNBC.

Nanodrug delivery systems (NDDSs) provide efficient approaches for the treatment of TNBC to improve drug treatment efficacy.[30] Recently, aggregation-induced emission (AIE) materials have emerged as attractive bioimaging tools due to their flexible controllability, negligible toxicity, and superior photostability.[31–33] AIE luminogens (AIEgens) exhibit highly bright fluorescence in the near-infrared (NIR) (700–900 nm) region and have have great application in the real-time visualization of biological processes with high temporal/spatial resolution and deep penetration, which make them ideal candidates for in vivo long-term tracking of NDDSs in a noninvasive manner.[34] Generally, the design of near-infrared AIEgens is focused on the donor–acceptor (D–A) structure, which contains alternate electron-donating and electron-withdrawing units because the adjustment of the push–pull effect involved in D–A structures has an advantage in making molecular emission colors tunable via the modification of the π-conjugated spacers. Previously, Dang et al reported a series of D–A type AIEgens employing triphenylamine derivatives as the donors, thiadiazolobenzotriazole as the acceptors, which not only displays high brightness in the near-infrared (NIR) emission region from 600 nm to 1000 nm (photoluminescence quantum yield, PLQYs=11.35%), but also displays excellent photo-stability.[35] These features endow thiadiazolobenzotriazole-cored AIEgens as ideal tracking agent for long-term visualization of drug delivery process in vivo.

In this study, we developed a chondroitin sulfate targeting nanodrug system (plCSA-NPs), which encapsulated thiadiazolobenzotriazole-cored NIR AIEgens (TBZ-DPNA) and therapeutic drug PTX, conjugated with plCSA as TNBC target peptide. We examined plCSA-NP binding activity and cytotoxicity on TNBC cell lines, and accessed anti-tumor effect on subcutaneous and lung metastatic tumor model.

Materials and Methods

Synthesis of Compound 4-(4-(Naphthalen-1-Yl(Phenyl) Amino) Phenyl)-Yl-8-Bromo-6-(2-Ethylhexyl)- [1,2,5] Thiadiazolo [3,4- F] Benzotriazole (TBZ-DPNA)

4.8-Dibromo-6-(2-ethylhexyl)- [1,2,5] thiadiazolo[3,4-f] benzotriazole was purchased from HWRK CHEM, and other chemicals were purchased from Sigma–Aldrich, J&K, TCI and used without further purification. Solvents and other common reagents were obtained from Sigma–Aldrich.

A solution of (4-(naphthalen-1-yl(phenyl) amino) phenyl) boronic acid(2) (339 mg, 1 mmol) in mixed solvent (20 mL, toluene: ethanol: water=18: 1: 1), 4.8-dibromo-6-(2-ethylhexyl)- [1,2,5] thiadiazolo[3.4-f]benzotriazole(3) (449 mg, 1.00 mmol), potassium carbonate (412 mg, 2.90 mmol) and tetrakis (triphenylphosphine) palladium(0) (116 mg, 0.2 mmol) was combined. The mixture was heated to 120 °C under a nitrogen atmosphere. After 8 h, the pale-yellow solution became purple-blue, and was removed from the heat. After cooling to room temperature, the solution was evaporated and purified by silica gel chromatography with petroleum ether/dichloromethane to yield TBZ-DPNA as a dark blue solid (460 mg, 70%).

Preparation of Nanodrug plCSA-NPs

A mixed solution of TBZ-DPNA (5 mg), DSPE-mPEG (10 mg), DSPE-PEG-COOH (10 mg), and PTX (5 mg) in THF (0.5 mL) was added rapidly to 5 mL phosphate-buffered saline (PBS) under ultrasonic conditions, and excess THF was then removed with nitrogen, for 5 minutes. Placental CSA-binding peptide (plCSA, EDVKDINFDTKEKFLAGCLIVSFHEGKC) and scrambled peptide (SCR, EVDNDKKLGLVFEKDKIFTEFACISHCG) were purchased from China Peptides Co., Ltd. (Shanghai, China). The peptides were conjugated to DSPE-PEG-COOH using EDC and NHS to activate the reaction with NH_2 from the peptide. Excess peptides and other impurities, such as EDC and NHS, were removed by triple filtration using AmiconUltra-4 centrifugal filters (MW10kD, Millipore, MA, USA) to obtain the final plCSA-conjugated nanoparticles (plCSA-NPs) and SCR-conjugated nanoparticles (SCR-NPs).

Characterization of plCSA-NPs

UV-vis absorption spectra were taken on a PerkinElmer Lambda 25 UV-Vis absorption spectrophotometer. Photoluminescence (PL) spectra were recorded with an Edinburgh F900 fluorescent spectrometer. Transmission electron microscope (TEM) images were taken on JEM 100CXII (JEOL). The TEM samples were prepared by placing a drop of plCSA-NPs solution onto a 300-mesh copper grid and then drying the sample at room temperature overnight. The particle sizes and zeta potential of particles were characterized on a Nano-Zetasizer (Nano ZS, Malvern, Malvern Instruments, USA) at 25 °C.

Cell Culture

The TNBC cell lines MDA-MB-231 and HCC1937, and the human mammary epithelial cell line MCF-10A were purchased from the American Type Culture Collection (ATCC). Cells were grown in DMEM (MDA-MB-231, HCC1937) supplemented with 10% FBS. MCF-10A cells were maintained in MEBM (Lonza) supplemented with 100 ng/mL cholera toxin (Sigma) and MEGM Single Quot (Lonza) supplemented with GA-1000 (gentamycin-amphotericin B mixture). All cell lines were maintained at 37 °C in a humidified atmosphere of 5% CO_2 before experiments.

Ethics Approval for Human Breast Cancer Tissue

Human breast cancer tissues involved this study were obtained from Peking University Shenzhen Hospital. The collection and use of human specimens were approved by the Institutional Review Board of Peking University Shenzhen Hospital and informed patient consent was given. All procedures in studies involving human participants were performed in accordance with the ethical standards of the institutional research committee and with the 1964 Declaration of Helsinki and its later amendments or comparable ethical standards. The collected breast cancer tissue was fixed in 4% paraformaldehyde (PFA) overnight for staining and molecular marker analysis.

Cellular Uptake and Cytotoxicity Assay

TNBC cell lines (MDA-MB-231, HCC1937) and human mammary epithelial cell lines (MCF-10A) were grown to 60% confluence in 12-well plates; these cell lines were treated with free NPs, SCR-NPs, or plCSA-NPs for 30 min. The cells were washed with PBS and fixed with 4% paraformaldehyde. After staining with DAPI, the cells were visualized under a fluorescence microscope (OLYMPUS IX71, Tokyo, Japan).

For cellular binding activity, MDA-MB-231, HCC1937 and MCF-10A cells were treated with 50 nM free NPs, SCR-NPs, or plCSA-NPs for 30 min. The cells were digested with trypsin and resuspended in PBS. All cell suspensions were analyzed with flow cytometer (BD, FACSAriaIII, USA).

MTT assay was performed to monitor the cytotoxicity of plCSA-NPs in vitro. MDA-MB-231 were seeded in 96-well plates (5×10^3 cells/well) for 24 h, starved with 0.04% FBS medium for another 12 h, and then treated with free PTX and NPs, SCR-NPs and plCSA-NPs with same amount of PTX concentration (from 5 nM to 50 nM) for 48 h. Cell viability was determined using the methylthiazole tetrazolium (MTT) method.

In vivo Imaging on Subcutaneous and Metastatic TNBC Models

Animal welfare and experimental procedures were approved by the Committee on the Use of Live Animals for Teaching and Research, Shenzhen Institutes of Advanced Technology, Chinese Academy of Sciences, and carried out in strict accordance with the related regulations. All applicable institutional guidelines for the care and use of animals were followed.

For subcutaneous tumor mouse model, 4- to 6-week-old female nude BALB/c mice were purchased from Beijing Vital River Laboratory Animal Technology Co., Ltd. (Beijing, China) and MDA-MB-231-labelled luciferase cells (1×10^6 cells in 100 μL Matrigel/mouse) were injected into the left axilla. After growth for one week, mice were randomly divided into three groups and tail veins were injected with 100μL of 1 mg/mL free NPs, SCR-NPs or plCSA-NPs.

The nanoparticle location on mice was measured with an IVIS spectrum instrument (Perkin Elmer) after treatment for 24 h with excitation (530 nm)/emission (780 nm). Mouse organs and tumor were collected to examine AIEgen with an IVIS spectrum instrument. For further study, tumor tissue was fixed with 4% PFA and sectioned to examine AIEgen with confocal laser scanning microscopy (TCS SP5, Leica, Hamburg, Germany).

Lung metastasis mouse model was established by tail vein injection of MDA-MB-231 cells labelled with luciferase and TOMATO (1×10^6 cells in 100 μL PBS/mouse). For one week of growth, mice were randomly treated with 100μL of 1 mg/mL free NPs, SCR-NPs, or plCSA-NPs for 24 h and imaged with the IVIS spectrum. From the sacrificed mice major tissues were collected to examine AIEdots accumulation. Lung tissue was fixed with 4% PFA and sectioned to measure colocalization with AIEdots and tumor cells (TOMATO).

In vivo Therapeutic Effect on Subcutaneous and Lung Metastatic TNBC Models

Subcutaneous and lung metastatic mouse model established as described in the last section. Following tumor growth for one week, mice were randomly divided into five groups (each group had 5–7 mice) and received saline, PTX, NPs, SCR-NPs and plCSA-NP treatments once every three days. Subcutaneous tumor length and width were measured with vernier calipers per week until day 30, and calculated tumor volume according to (length) × (width) $^2\times0.5$. Tumor growth was also determined with luciferin imaging with IVIS spectrum. Tumors were collected and measured for weight, then fixed for staining examination. Lung metastatic tumor was also monitored with the IVIS spectrum and lungs were excised and fixed for further examination.

Tumor Staining

The excised subcutaneous tumor was placed in paraffin. After sectioning, staining against CD31 (Abcam, ab15580) was performed with an immunohistochemistry kit (Key-GEN, Nanjing, China). For the TUNEL assay, the fragEL DNA Fragmentation Detection Kit (Calbiochem, Germany) was used to detect apoptotic cells in tumor tissue. The number of stained positive cells was calculated with 8–10 vision and quantified as the mean cell number. Lung tissues from metastatic model were stained with DAPI to examine tumor cell marker TOMATO location under fluorescence microscope.

Serum Biochemistry Assay and HE Staining

Blood samples were collected from mice in therapeutic subcutaneous and lung metastatic mouse models and the ALT, AST, ALP and GCT activity was detected using an automated hematology analyzer. Liver and kidney organs from these two mouse models were embedded in paraffin and examined by hematoxylin and eosin (H&E) staining.

Flow Cytometry for Mixed Lymphocytes with TNBC

Mouse blood samples were collected in tubes, and lymphocytes were isolated with lymphoprep gradient. Lymphocytes were mixed with MDA-MB-231 in a 1:1 ratio and incubated with 50 nM FITC-plCSA and PE-CD45 antibody for 30 min at 4 °C. Following three wash steps in PBS with 2% FBS, the cell mixture was examined with an FC500 flow cytometer (Beckman Coulter), and the cell percentages of FITC- or PE-positive cells were analyzed. After that, the mixture of MDA-MB-231 cells with lymphocytes was flipped on glass slides and stained with DAPI for nuclei, and plCSA-binding breast cancer cells and CD45-binding lymphocytes were observed by microscopy (Olympus BX53, Japan).

Statistics

All the results are presented as the mean±SD of at least three independent experiments. Statistical analyses were performed with one-way ANOVA (GraphPad Prism 8.0) for multiple groups. The threshold of $p < 0.05$ was defined as statistically significant.

Results

Rational Design and Optical Properties of TBZ-BPNA

Typically, the integration of strong electron donor–acceptor (D–A) interactions into conjugated structured chromophores could remarkably facilitate intramolecular charge transfer (ICT) and conjugation length. In this study, the molecule was easily synthesized and purified by a one-step Suzuki reaction with a high yield (Figure 1A). Chemical structure was characterized and confirmed by NMR and high-resolution mass spectrometry (HRMS) (Figures S1 and S2). In this structure, the thiadiazolo-benzotriazole moiety (TBZ, red) acts as the acceptor, and N, N-diphenylnaphthalen-1-amine (DPNA, blue) acts as the donor to form a strong D–A interaction. To investigate the optical properties of TBZ-DPNA, UV–vis and photoluminescence (PL) spectra in tetrahydrofuran (THF) were recorded, as shown in Figure 1B, which exhibited absorption maxima at 330 nm and 584 nm, respectively, and maximum emission feature was located at 718 nm. Furthermore, the AIE properties of TBZ-DPNA were also confirmed by studying its PL spectra in water/DMSO mixtures with different water volume fractions, as shown in Figure 1C. When the water fraction was lower than 60%, the emission of TBZ-DPNA was rapidly quenched due to the twisted intramolecular charge transfer (TICT) effect. The water fraction exceeded 60% and the PL intensity was enhanced because the energy consumption of the excited state was reduced by restrained intramolecular motions.

In vitro Targeting and Cytotoxicity Activity Analysis for Nanodrug plCSA-NPs

First, we synthesized peptides plCSA and SCR to access targeting activity on TNBC cell lines and TNBC tumor tissue. Flow cytometry and binding assay showed plCSA specifically combined with TNBC tumor and MDA-MB-231 and HCC-1937 cells (Figures S3 and S4). Next, nanoparticles (NPs) were synthesized with PLGA, soybean lecithin, and DSPE-PEG-COOH using a single-step sonication method, which loaded TBZ-BPNA and therapy drug PTX. SCR and plCSA then conjugated with NPs through the amino terminus of the peptide to carboxyl groups on the surfaces of nanoparticles to produce SCR-NPs and plCSA-NPs (Figure S5). Photophysical properties of plCSA-NPs, as shown in Figure 2A, displayed absorption at 589 nm and maximum emission peak at 747 nm with strong fluorescence intensities mainly located in the NIR region. The morphology and size measurement of plCSA-NPs showed a nearly monodispersed nanosphere morphology with an average diameter of 70 nm, as measured with dynamic light scattering (DLS) and transmission electron microscopy (TEM) imaging (Figure 2B and C).

To evaluate the targeting activity of plCSA-NPs on TNBC cell lines, MDA-MB-231, HCC1937 and the human normal mammary epithelial cell line MCF10A were incubated with 50 nM NPs, SCR-NPs or plCSA-NPs for 4 h. Both

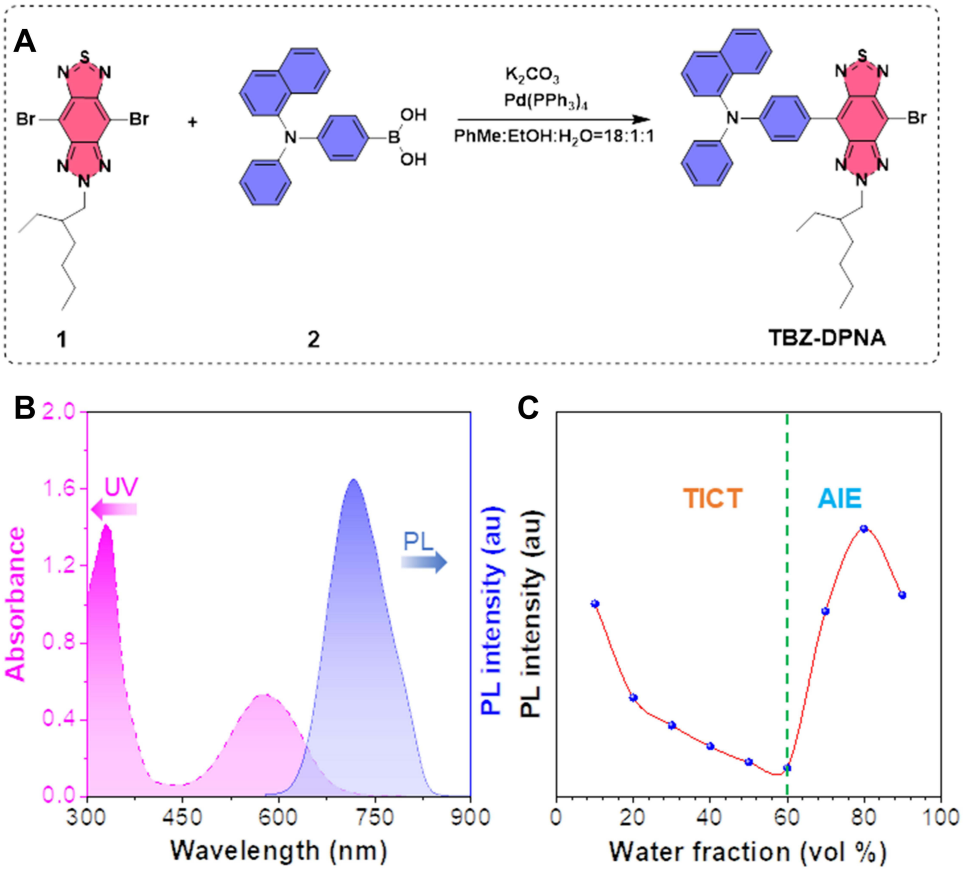

Figure 1 Design synthesis and optical properties of TBZ-BPNA. (**A**) Synthetic route of TBZ-BPNA. (**B**) Absorption and emission spectra of TBZ-BPNA in THF solution. (**C**) Plot of PL intensity of TBZ-BPNA at maximum emission wavelength vs the water fraction in the water/DMSO mixtures.

MDA-MB-231 and HCC1937 showed increased fluorescence signals on plCSA-NP-treated group (Figure 2D). Consistently, plCSA-NP treatment led to aggregated AIEdots accumulation on TNBC cells, most of which located on lysosomes (Figure S6). In contrast, little AIEdots was observed on MCF10A, indicated plCSA-NPs did not interact with normal human epothelial cell of mammay (Figure 2D). The cytotoxicity of plCSA-NPs was performed on MDA-MB-231 cells with PTX and same concentration of NPs, SCR-NPs and plCSA-NPs. plCSA-NPs showed significant cell toxicity, while approximately 50% of cells were dead when cultured with plCSA-NPs on 50 nM PTX. However, PTX, NPs and SCR-NPs on this concentration had little effect on cell viability (Figure 2E). Overall, these data provided solid data for plCSA-NP's targeting and cytotoxicity activity to TNBC cell lines.

Biodistribution for plCSA-NPs in Subcutaneous Mouse Model

A mouse subcutaneous tumor model was established with female nude mice injected with MDA-MB-231 cells into the left axilla. When the tumor grew for one week, nanoparticles were administered by intravenous injection. The fluorescence of whole animal imaging was used to investigate the tumor targeting and nanoparticle distribution (Figure 3A); NP and SCR-NP treatments were used as controls. As indicated, the fluorescence signal from plCSA-NPs accumulated on tumor site and signal intensity gradually increased; signal peak occurred at 8 h, and until 24 h showed no attenuation compared to the NPs and SCR-NPs (Figure 3B). At 24 h post-injection, ex vivo tumor and organs were dissected and examined using fluorescence signal accumulation (Figure 3C). As indicated in Figure 3D, plCSA-NP promoted AIEdots aggregation on tumor compared to NPs and SCR-NPs, which was further confirmed by AIEdots deposition in tumor tissue (Figure 3E). These data suggested that plCSA-NPs positively targeted TNBC subcutaneous tumors.

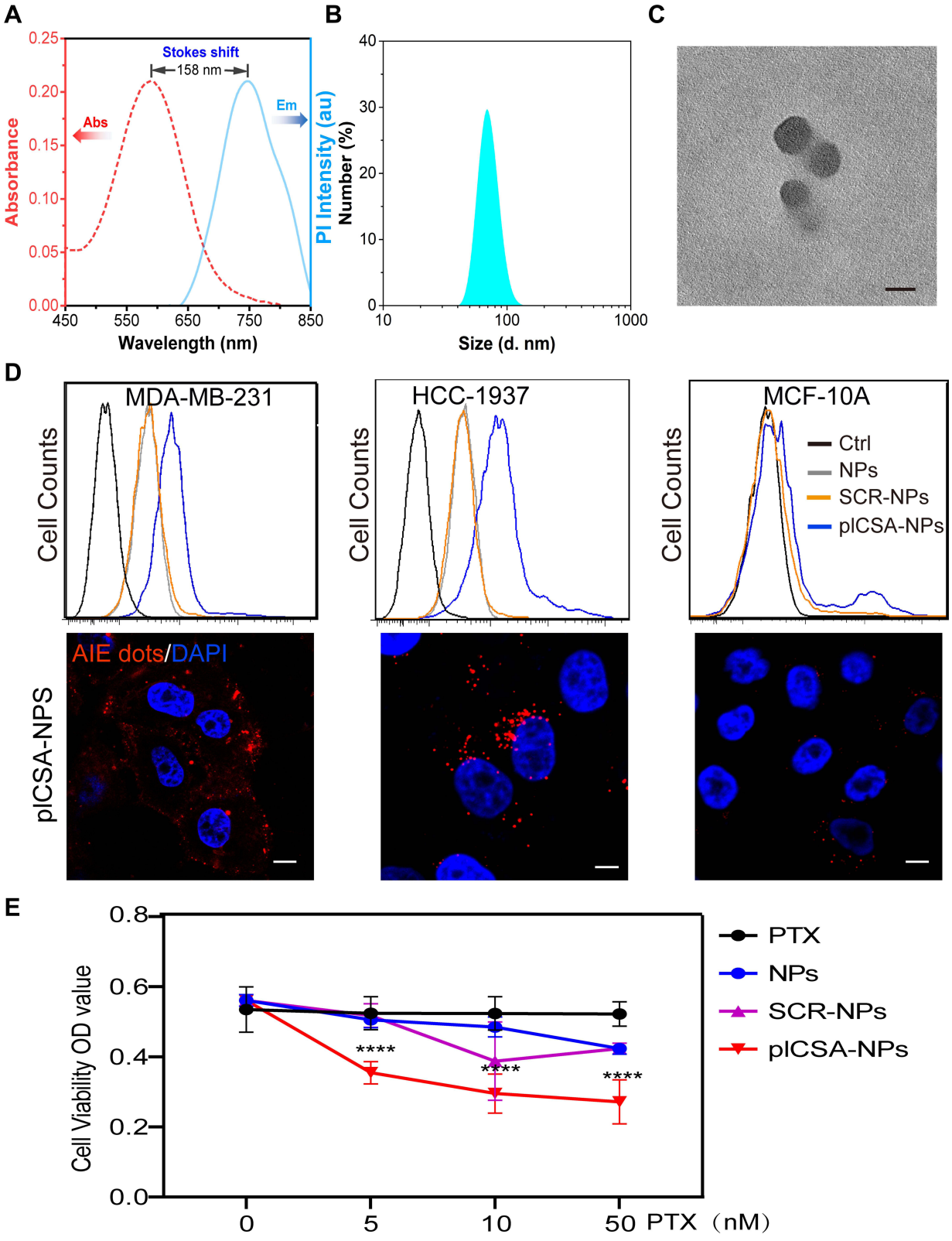

Figure 2 Cellular uptake and cytotoxicity assay for pICSA-NPs. (**A**) Absorption and PL spectrum of pICSA -NPs in water. (Ex=589 nm) (**B** and **C**) Size measurement of pICSA-NPs, scale bars=50nm. (**D**) Representative flow cytometry histograms of fluorescence curves for MDA-MB-231, HCC1937 and MCF10A after exposed 50nM NPs, SCR-NPs or pICSA-NPs. The aggregated AIEdots of pICSA-NPs also observed on cellular cell, scale bars=20μm. (**E**) Proliferation curve of MDA-MB-231 exposed to PTX, NPs, SCR-NPs or pICSA-NPs with PTX concentration from 5nM to 50nM for 24h. **** indicates $p \leq 0.0001$ by one-way ANOVA with post hoc Tukey.

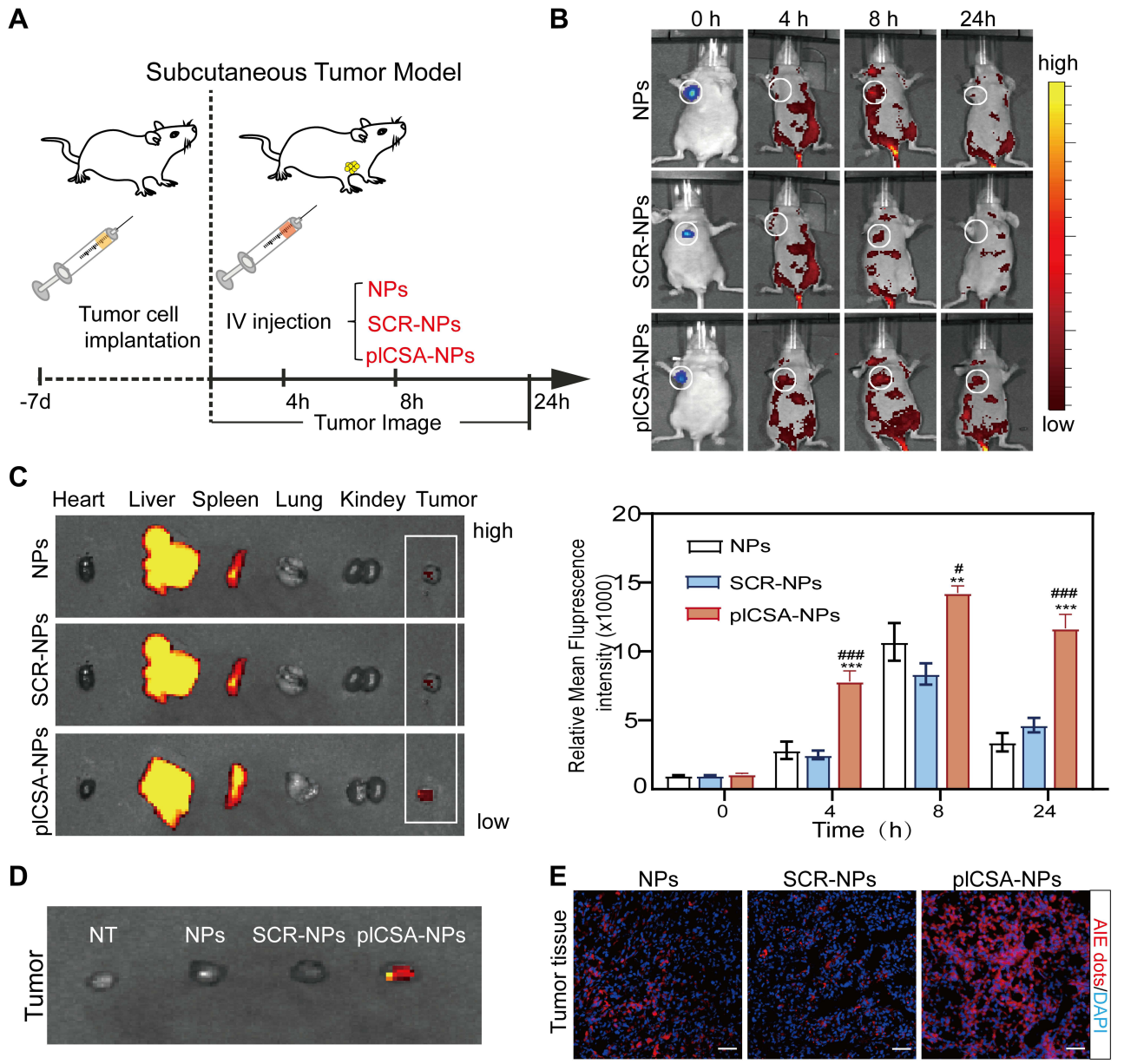

Figure 3 Biodistribution of plCSA-NPs in subcutaneous mouse model. (**A**) The scheme illustrates the process plCSA-NPs on TNBC subcutaneous tumor model. (**B**) Representative fluorescence images of nude mice bearing luciferase-MDA-MB-231 subcutaneous tumors intravenously injected with NPs, SCR-NPs or plCSA-NPs with IVIS spectrum imaging system. Circles point out the region of interest (ROI) where fluorescence intensity is measured. The relative mean fluorescence signal intensity of AIE in subcutaneous MDA-MB-231 tumors in mice 0, 8, and 24 h post-intravenous injection of 100 μL 1mg/mL NPs, SCR-NPs or plCSA-NPs (n=4). (**C** and **D**) AIEdots distribution on the main organs (heart, liver, spleen and kidney) and tumor tissues. (**E**) The representative image for AIEdots accumulation on tumor tissue, scale bars=100μm. Statistical significance calculated methods using the one-way ANOVA. **p <0.01, ***p <0.001 versus NPs group, $^{\#}$p ≤0.05 and $^{\#\#\#}$p ≤0.001 versus SCR group.

plCSA-NPs Inhibited TNBC Subcutaneous Tumor Growth

The CCK-8 test was used to evaluate the therapeutic effect of plCSA-NPs on tumor growth in vitro. As the concentration of plCSA-NPs added to TNBC cell lines, the cell proliferation was inhibited. The xenograft mouse model was established as described in Figure 3A. After tumor growth for one week, plCSA-NPs was administered to tumor-bearing mice by intravenous injection for one to three days. After treatment for 30 days, the tumor volume and imaging data showed decreased tumor growth in plCSA-NP-treated groups (Figure 4A), which was further confirmed by the smaller size and lower weight of tumor (Figure 4B). Accordingly, increased apoptosis in tumor cells and decline in vessel formation were observed in plCSA-NP-treated tumor (Figure 4C). In addition, the mouse body weights and H&E staining results showed

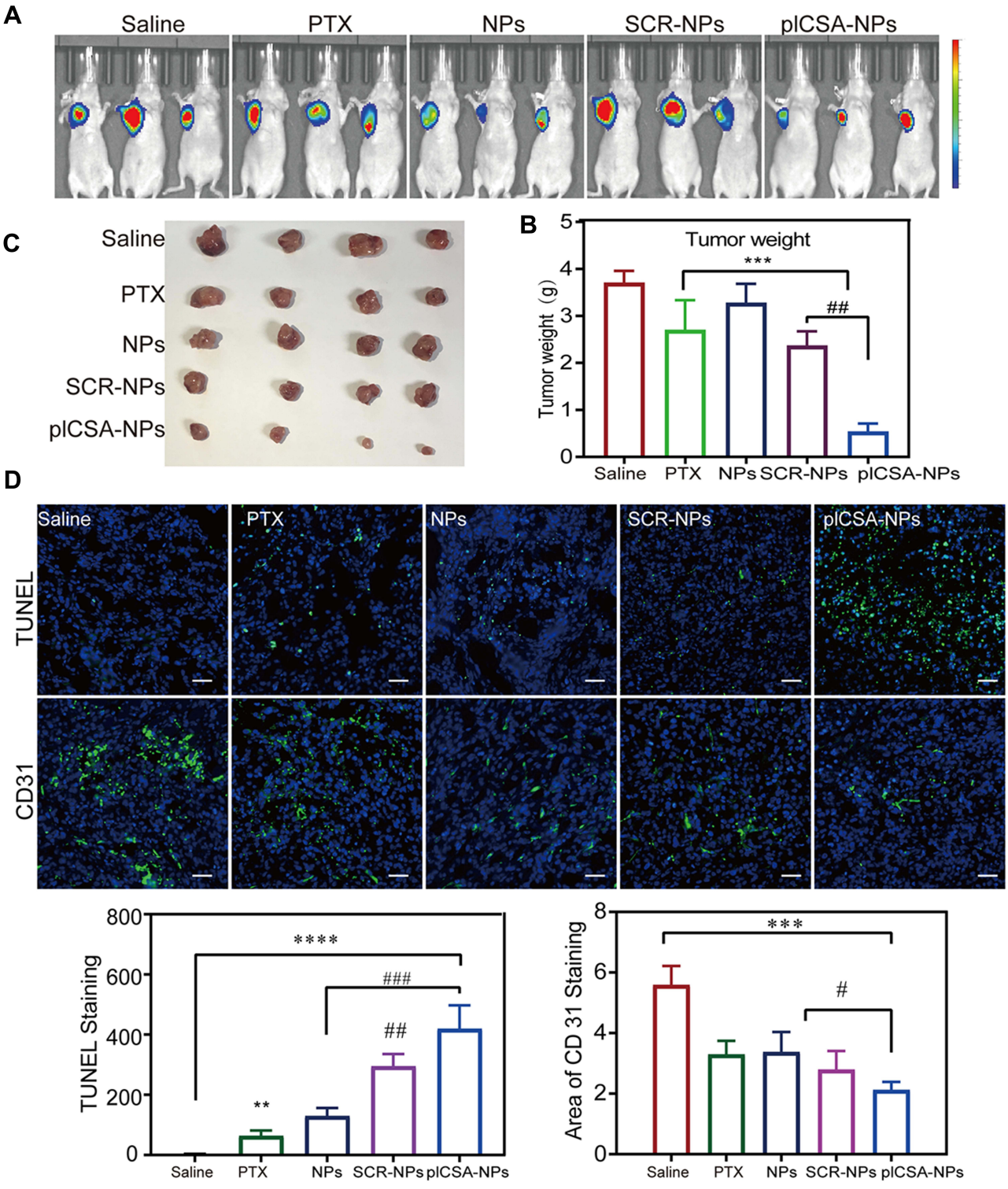

Figure 4 Inhibitory effects of plCSA-NPs against subcutaneous TNBC tumor. (**A**) The tumor image of subcutaneous tumor model after intravenously injected saline, free PTX, NPs, SCR-NPs, or plCSA-NPs for 30 days (5 mg/kg PTX equivalent) (each group with 5 mice). (**B**) Caliper measurements of tumor sizes and calculated tumor volume in mice after the intravenous injection of nanoparticle every three days (data represent the mean±SD). (**C**) Tumor volume and tumor weight were presented after mice sacrificed. (**D**) Tunnel assay and CD31 staining performed on tumor tissue section and presented as representative image, scale bars=50μm. The apoptosis cell numbers and CD31 staining areas were calculated from 8–10 version for each mouse tissue. $^{**}p \leq 0.01$, $^{***}p \leq 0.001$, $^{****}p \leq 0.0001$, $^{\#}p \leq 0.05$, $^{\#\#}p \leq 0.01$, $^{\#\#\#}p \leq 0.001$ were calculated with the one-way ANOVA.

no obvious organ damage from nanoparticle treatment (Figure S7). Therefore, we concluded that plCSA-NPs inhibited TNBC tumor growth.

plCSA-NPs Targeting Activity on TNBC Tumor in the Lung

To explore the role of plCSA-NPs on TNBC metastasis, a lung metastatic model was established with tail vein injection of MDA-MB-231 cell-labelled luciferase and TOMATO (Figure 5A). When grown for one week, tumor could be observed on the mouse lung site, then plCSA-NPs were administered to mice via tail vein injection. We examined fluorescence signal at 4 h, 8 h and 24 h (Figure 5B); similar to subcutaneous tumor, plCSA-NPs significantly accumulated on lung tumor site compared to NPs and SCR-NPs groups (Figure 5C and D). Furthermore, we examined AIEdots and TOMATO signals (labelled for tumor cells) in lung tissue sections. A lot of AIEdots aggregated around tumor cells in plCSA-NP group, while few could be observed in NP and SCR-NP groups (Figure 5E). These results suggested that plCSA-NPs had the ability to target TNBC lung metastatic tumor.

plCSA-NPs Suppressed TNBC Tumor Growth in the Lung

Inspired by the results of plCSA-NPs on TNBC metastatic tumor, we investigated the therapeutic activity of plCSA-NPs on TNBC metastasis. As mentioned in the last section, lung metastatic mouse model was established with tail vein injection of MDA-MB-231-TOMATO cells into 4-week-old nude female mice. After growth for 7 days, plCSA-NPs were treated via the tail vein every one to three days for 30 days. Tumor growth showed PTX alone; NP or SCR-NP groups had similar growth curves to those of the saline group, suggest these treated group had little effect on metastatic tumor. By comparison, plCSA-NP group significantly suppressed metastatic tumor growth, but had no effect on mouse weight (Figure 6A-C). Tumor growth in lung tissue was further examined with TOMATO. The results showed that the saline, PTX, NP and SCR-NP groups had tremendous tumor burden in lung tissue, while the plCSA-NP group had much smaller tumor, as indicated by TOMATO (Figure 6D), suggesting that plCSA-NPs had anti-tumor effect on lung metastasis.

Toxicology Analysis for plCSA-NPs

To further investigate the potential toxicology of plCSA-NPs, each treated group from the lung metastatic mouse model was subjected to a serum biochemistry assay and histological examination of liver and kidney tissue sections. The liver function indicators, including alanine aminotransferase (ALT), aspartic acid transaminase (AST), alkaline phosphatase (ALP) and γ-globulin transferase (GGT), were all found to be normal (Figure 7A) and revealed no obvious hepatic disorders in plCSA-NP-treated mice. In addition, the histological examination of liver and kidney tissue sections (Figure 7B) displayed a similar architecture to that in the saline group, with intact hepatic cords, fewer inflammatory cells around the central vein, less hepatocyte necrosis, and fewer activated Kupffer cells. Further, we verified biocompatibility of plCSA-NP by hemolysis test (Figure S8) and, combined with negligible influences of plCSA-NPs on mouse body weight (Figure 6C), it is reasonable to conclude that plCSA-NPs was a biocompatible nanodrug with no noticeable side effects in living mice.

Distinguishing Metastatic TNBC Cells from Peripheral Circulation

In the clinic, approximately two-thirds of TNBC patients treated with neoadjuvant chemotherapy will relapse and develop metastasis.[36] Dissemination of TNBC cells through blood circulation is an important intermediate step that represents the switch from localized to systemic disease.[37,38] Early detection and characterization of circulating tumor cells (CTCs) is therefore important as a general strategy to check and prevent the development of overt TNBC metastatic disease.[39,40] Although our results show the great potential of plCSA-NPs to clean up metastatic TNBC tumor, we attempted to evaluate their effect on circulated TNBC. In this experiment, we collected lymphocyte cells from peripheral circulation, mixed MDA-MB-231 with ratio of 1:1, and performed flow cytometry with FITC-plCSA and PE-CD45 to distinguish TNBC and lymphocytes. We incubated cell mixture with FITC-SCR or FITC-plCSA with PE-CD45 together for 30 min and flow cytometry results showed plCSA 31% binding activity with MDA-MB-231 31%, compared to Ctrl and SCR groups 0.116% and 0.265% (Figure 8A). In contrast, the CD45 combined lymphocyte percentage was not

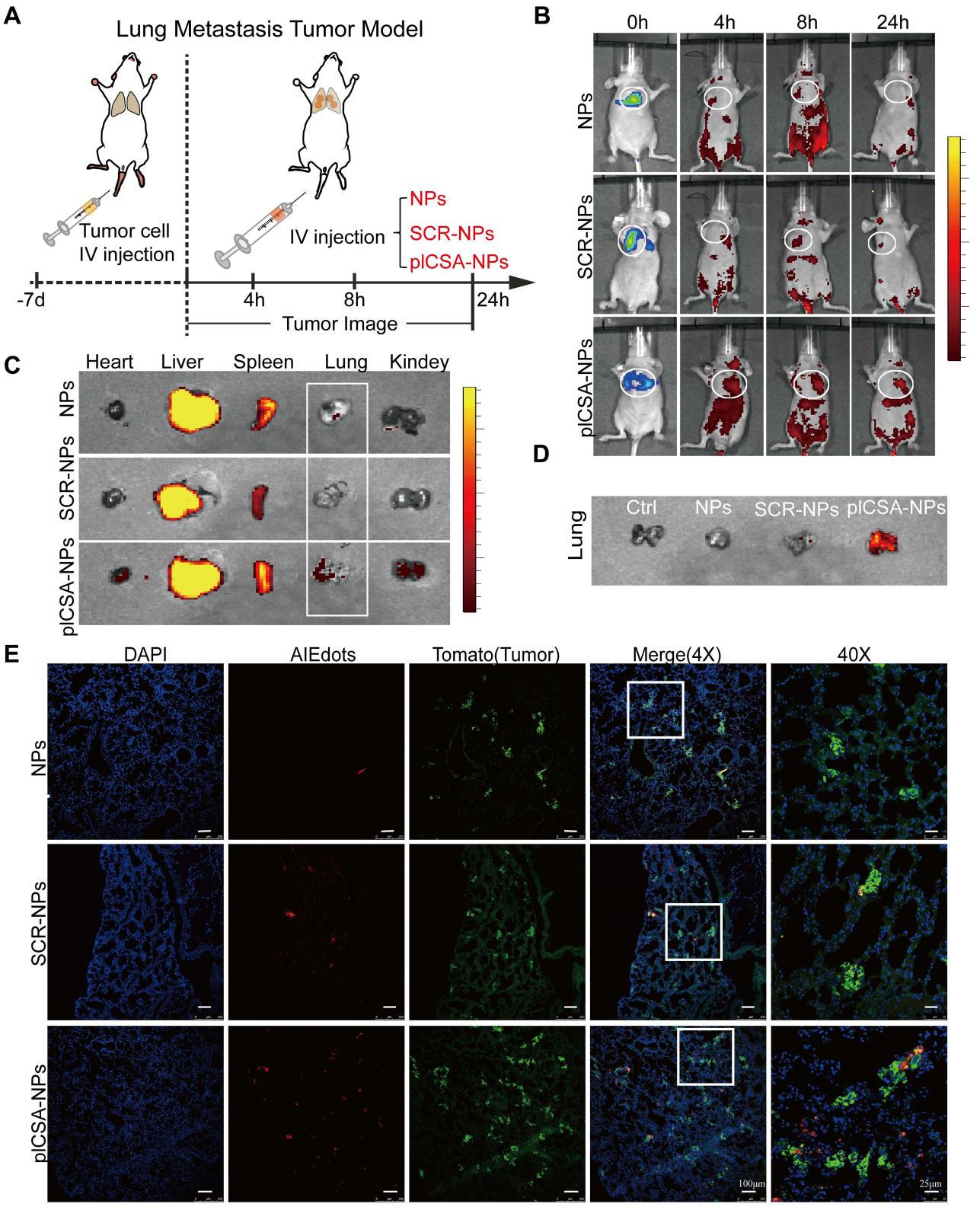

Figure 5 plCSA-NPs targeting activity on TNBC tumor in the lung. (**A**) The scheme illustratiing the process of nude mice lung metastasis model intravenously injected with 100 μL 1mg/mL NPs, SCR-NPs or plCSA-NPs. Mice monitored tumor sites after 24 h using IVIS spectrum imaging system. (**B**) Representative AIEdots image on lung metastatic tumors after intravenously injected with NPs, SCR-NPs or plCSA-NPs. Circles point out the region of interest (ROI) where fluorescence intensity measured. The relative mean fluorescence signal intensity of AIE in mice 0, 8, and 24 h post-intravenous injection of 100 μL 1mg/mL NPs, SCR-NPs or plCSA-NPs (n=4). (**C** and **D**) AIEdots distribution on the main organs (heart, liver, spleen, kidney and lung). (**E**) AIEdots distribution (red) and tumor cell (TOMATO, green) location on lung tissue; scale bars=100μm for 4X and scale bars=25 μm for 40X.

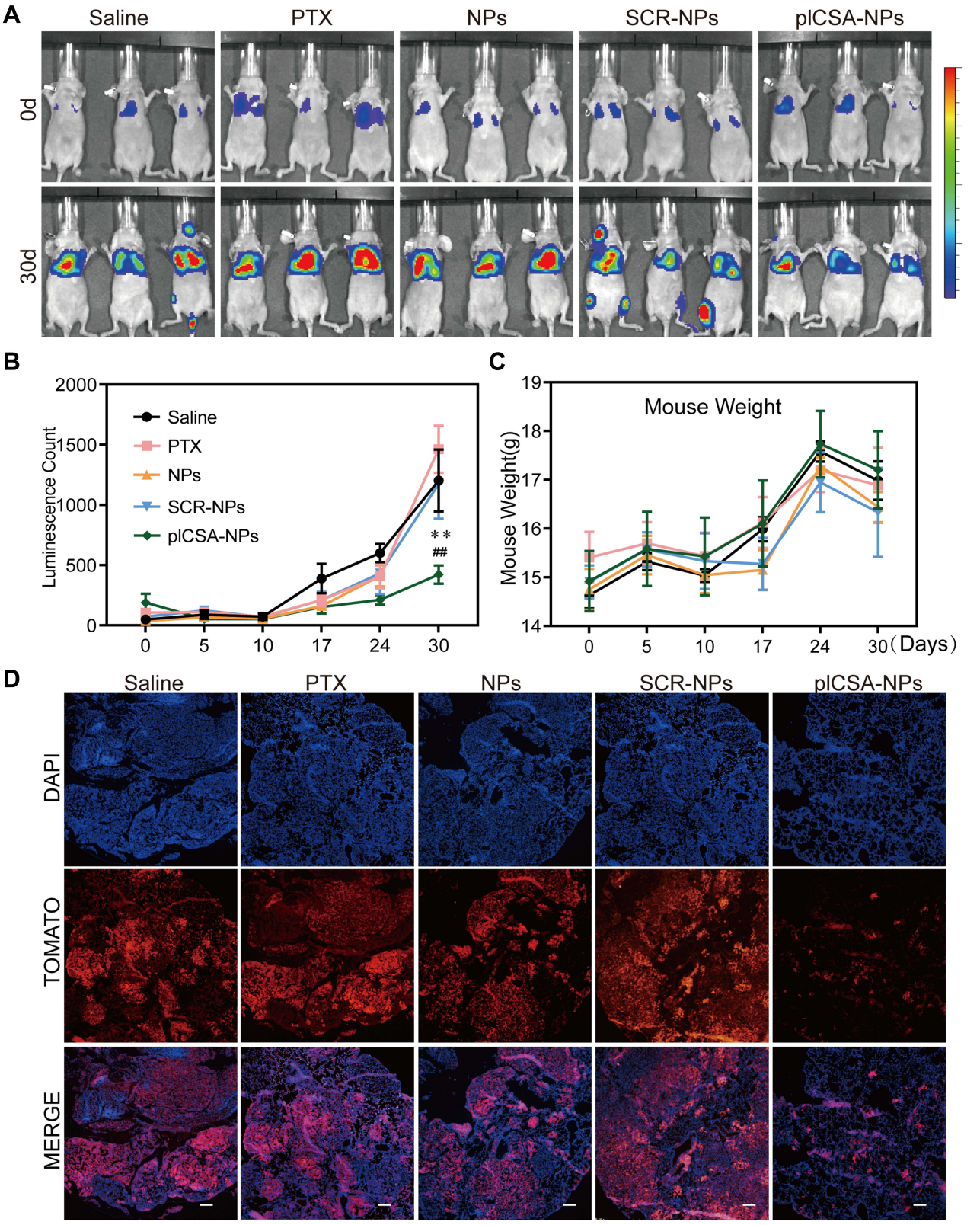

Figure 6 plCSA-NPs suppresses TNBC lung metastatic tumor growth. (**A**) The representative tumor image on lung metastasis mice model with intravenous injection of saline, free PTX, the NPs, SCR-NPs, or plCSA-NPs (5 mg/kg PTX equivalent) for 30 days. (**B**) Quantification of the IVIS signal from metastasis tumor cell at different time intervals from days 0 to 30 after injection. (**C**) Mouse weight of each group after treatment. (**D**) Lung tissues were sectioned after mice scarified and tumor growth was examined with TOMATO signal. The version is representative image from microscopy on 4X; scale bars=50 μm. **p ≤0.01 (with PTX group) and ##p ≤0.01 (with NPs group) were calculated with the one-way ANOVA.

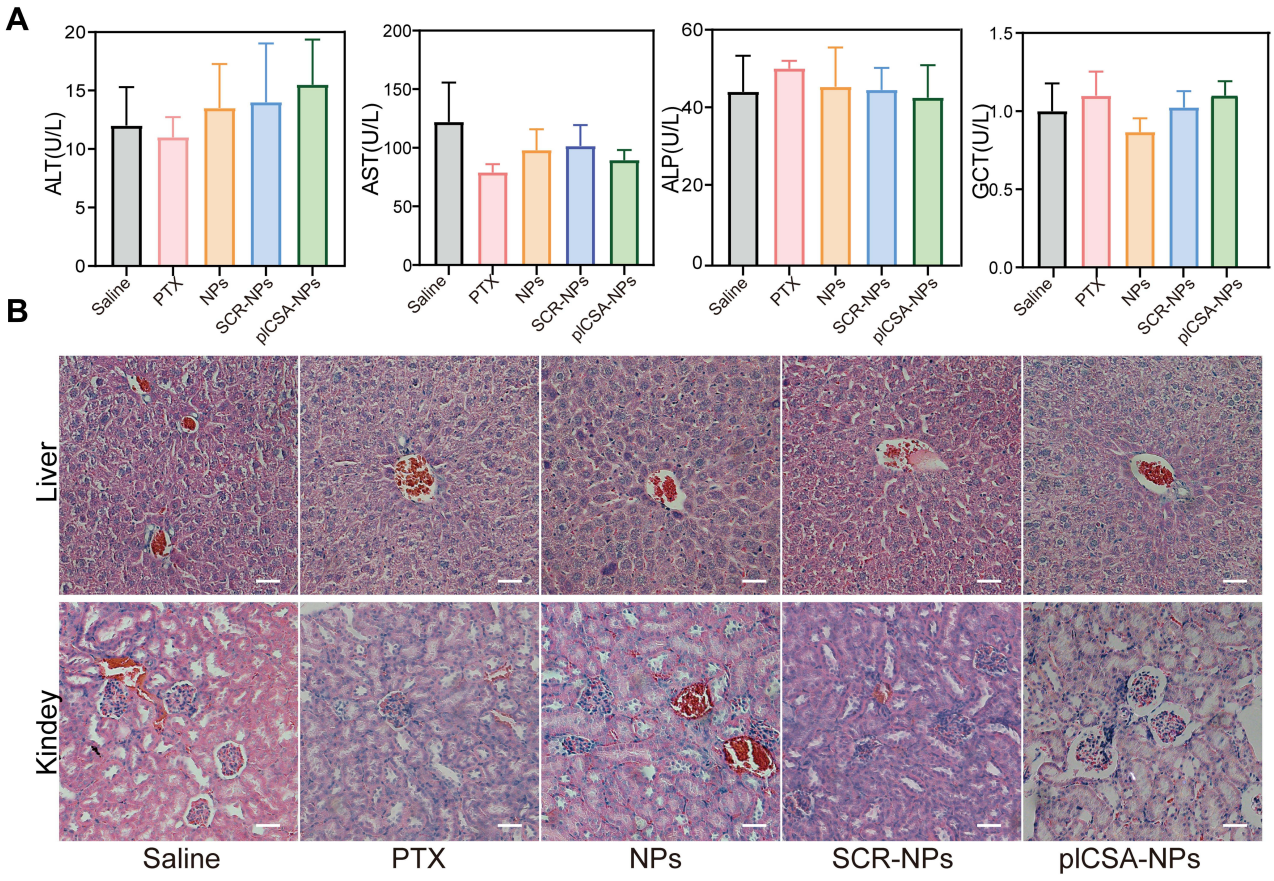

Figure 7 Toxicities of plCSA-NPs on lung metastatic mouse. (**A**) Blood test parameters in terms of liver function of each treated group on lung metastasis mouse. The saline mice were used as the control. (**B**) HE staining for liver (upper panel) and kidney tissue (lower panel) for renal and hepatic toxicity; scale bars=50 μm.

significantly changed in these three groups. These results were observed in the HCC1937 cell line; plCSA binding activity was approximately 32% with HCC1937 cells, while the SCR and Ctrl groups were only 9.27% and 5.44%, respectively (Figure S9). Following these results, FITC-plCSA-treated cell mixture examined under a microscope readily indicated tumor cells (FITC labelled) in background of normal CD45-positive lymphocytes (red) (Figure 8B). These results indicated that plCSA-NPs had the ability to clean up tumor cells in the circulation to block TNBC metastasis.

Discussion

Triple-negative breast cancer (TNBC) is more aggressive than other subtypes, has a poor prognosis and more potential to metastasize to other tissues, which dramatically reduces the overall survival rate of patients.[41] Lack of well-defined molecular targets is a big obstacle to treating TNBC.[42,43] Here, our results suggested a TNBC targeted nanodrug delivery system, plCSA-NPs, which achieved: (I) recognized TNBC tumor cells and captured circulated TNBC in peripheral circulation; (II) surveillance of primary and metastatic tumor growth in a non-invasive manner; (III) successfully delivered therapeutic drug PTX to subcutaneous and lung metastatic TNBC cells and inhibited tumor growth. Overall, our results provided a promising TNBC targeting nanodrug delivery system for TNBC treatment.

There are several reasons to choose oncofetal chondroitin sulfate for the TNBC therapeutic targeting. First, placenta CSPG is a distinct CSA subtype only expressed on placental syncytium[44] and cancers tissue include breast tumor.[20] Our synthesized peptide plCSA has high affinity with CSA(KD~15 nM)[26] on tumor tissues.[29,45] Primary results provided solid data that plCSA had little bind activity with human mammary epithelial cells, but high affinity with TNBC cells and tumor tissues (Figures S3 and S4). Second, oncofetal chondroitin sulfate on tumor surface undergoes constitutive internalization when bound by anchor protein VAR2CSA,[23] which was further confirmed by

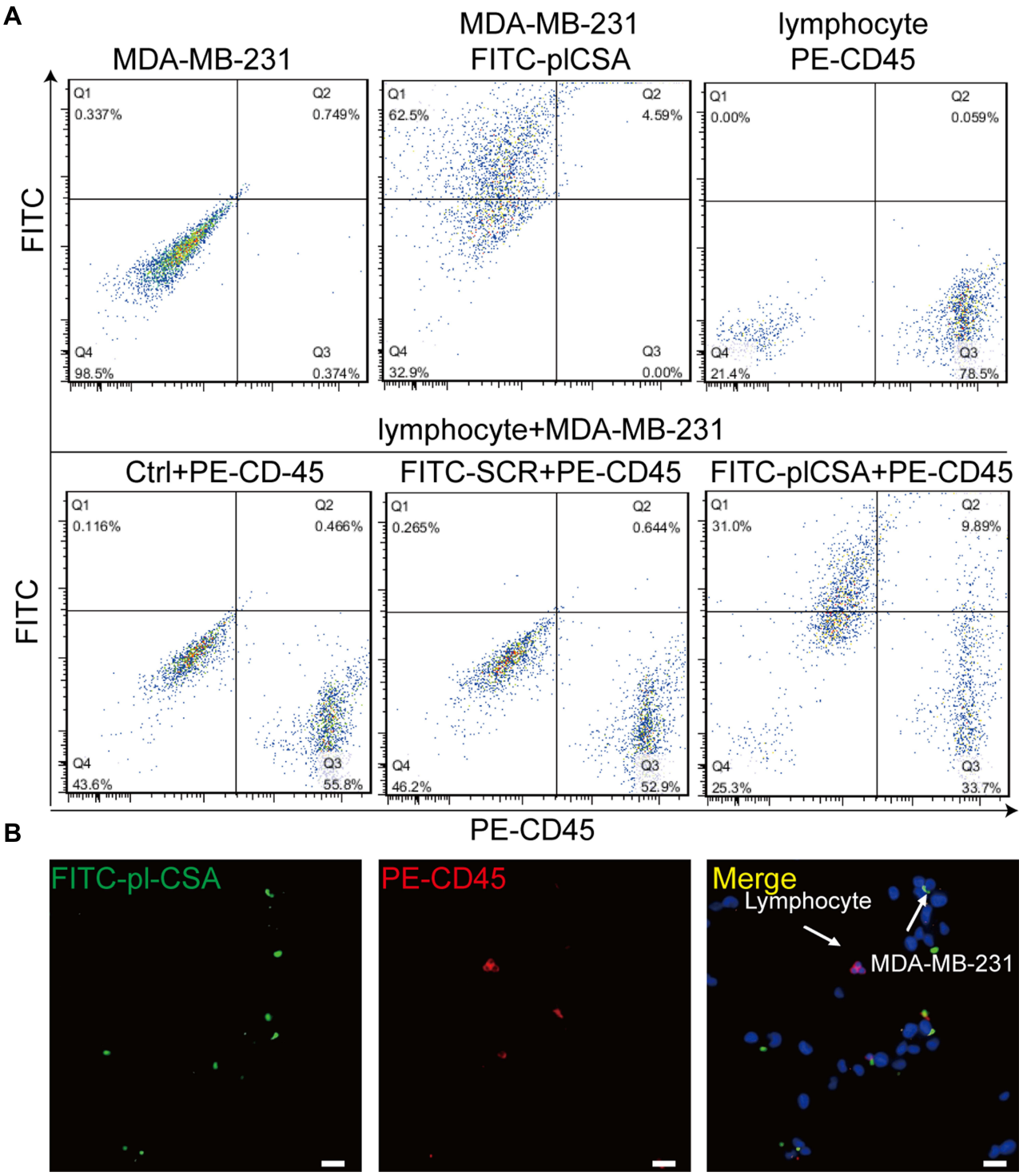

Figure 8 plCSAs' ability to distinguish TNBC cells from peripheral circulation. (**A**) The flow cytometry was performed to examine fluorescence of FITC-plCSA (y-axis) with PE-conjugated anti-CD45 antibody (x-axis). The image is the representative result for three times. (**B**) MDA-MB-231 cells were mixed with PBMCs in a 1:1 ratio and stained with FITC-plCSA (green), PE-CD45 antibody (red) and DAPI (blue). Scale bars=10 μm.

plCSA-NPs cellular uptake and cytotoxicity on MDA-MB-231 and HCC-1937 (Figure S6). Our study showed that plCSA-NPs' anti-tumor effect on TNBC tumors and metastatic tumors in lungs is likely dependent on binding with oncofetal chondroitin sulfate on TNBC surface and then endocytosis of nanoparticles. Third, plCSA is small peptide with 28 amino acids, easily synthesized and conjugated on surface. plCSA-NPs will be more efficient than other

target systems like mAb in escaping systemic clearance.[46] In addition, we suggested plCSA as a tool to enrich circulated TNBC from peripheral blood, to play a role on clean-up of tumor cells in the circulation or capture of tumor cells for diagnosis of molecular residual disease (MRD).[47] Taken together, we believe that plCSA may be a more effective tumor cell target for nanoparticle delivery to TNBC tumors compared to other cell surface proteins.

Aggregation-induced emission (AIE) materials have great potential for non-invasive NIR fluorescence image-guided therapy for TNBC and TNBC metastasis.[48,49] Here, our designed NIR AIEgens TBZ-DPNA, based on a donor−acceptor (D−A) architecture, access molecules with an intramolecular charge-transfer (ICT) excited state and deeply red-shifted absorption and emission bands.[50,51] This probe excites near-infrared (NIR) dyes at wavelengths from 700 to 1000 nm and provides high-contrast images to trace TNBC subcutaneous and metastatic tumor growth. More importantly, AIEgens involving photodynamic therapy (PDT) has emerged as a novel, non-invasive and safe treatment, causing minimal damage and with few side effects to widely investigate in TNBC therapy.[52,53] This part was not supported by the current study and we have planned for the next study to optimize particles and investigate PDT on TNBC tumors.

Conclusion

In summary, our study suggests a promising TNBC targeting nanodrug delivery system, which achieved good targeting efficiency and therapeutic effects against TNBC subcutaneous and lung metastatic tumor growth.

Acknowledgments

This work was supported by National Key R&D Programs (2021YFA0910000), National Nature Science Foundation of China grant (NSFC) (81901509), Shenzhen grant (JCYJ20190812165809537, JCYJ20210324120011030, JCYJ20220531095811025, JCYJ20220818101218040) and Shenzhen Key Laboratory of Metabolic Health (ZDSYS20210427152400001). The corresponding author Jian V. Zhang had final responsibility for the decision to submit for publication.

Disclosure

The authors report no conflicts of interest in this work.

References

1. Denkert C, Liedtke C, Tutt A, von Minckwitz G. Molecular alterations in triple-negative breast cancer-The road to new treatment strategies. *Lancet*. 2017;389(10087):2430–2442. doi:10.1016/S0140-6736(16
2. Hamann U, Ankel C. Breast Cancer: diagnostics and Therapy - The Most Important Facts for Internists. *Deut Med Wochenschr*. 2018;143 (4):267–276. doi:10.1055/s-0043-104456
3. Weigelt B, Peterse JL, van 't Veer LJ. Breast cancer metastasis: markers and models. *Nat Rev Cancer*. 2005;5(8):591–602. doi:10.1038/nrc1670
4. Sari E, Yalcin S. Clinical Aspects of Estrogen and Progesterone Receptors and ERBB2 Testing. *Breast Dis*. 2016;1:854 doi:10.5455/medarh.2018.72.335-340.
5. Bauer KR, Brown M, Cress RD, Parise CA, Caggiano V. Descriptive analysis of estrogen receptor (ER)negative, progesterone receptor (PR)-negative, and HER2-negative invasive breast cancer, the so-called triple-negative phenotype - A population-based study from the California Cancer Registry. *Cancer*. 2007;109(9):1721–1728. doi:10.1002/cncr.22618
6. Duffy MJ, McGowan PM, Crown J. Targeted therapy for triple-negative breast cancer: where are we? *Int j Cancer*. 2012;131(11):2471–2477. doi:10.1002/ijc.27632
7. Swain SM, Kim SB, Cortes J, et al. Pertuzumab, trastuzumab, and docetaxel for HER2-positive metastatic breast cancer (CLEOPATRA study): overall survival results from a randomised, double-blind, placebo-controlled, Phase 3 study. *Lancet Oncol*. 2013;14(6):461–471. doi:10.1016/S1470-2045(13)70130-X
8. Brewster AM, Chavez-MacGregor M, Brown P. Epidemiology, biology, and treatment of triple-negative breast cancer in women of African ancestry. *Lancet Oncol*. 2014;15(13):e625–e34. doi:10.1016/S1470-2045(14)70364-X
9. Bianchini G, Balko JM, Mayer IA, Sanders ME, Gianni L. Triple-negative breast cancer: challenges and opportunities of a heterogeneous disease. *Nat Rev Clin Oncol*. 2016;13(11):674–690. doi:10.1038/nrclinonc.2016.66
10. Garrido-Castro AC, Lin NU, Polyak K. Insights into Molecular Classifications of Triple-Negative Breast Cancer: improving Patient Selection for Treatment. *Cancer Discov*. 2019;9(2):176–198. doi:10.1158/2159-8290.CD-18-1177
11. Carey LA, Dees EC, Sawyer L, et al. The triple negative paradox: primary tumor chemosensitivity of breast cancer subtypes. *Clin Cancer Res*. 2007;13(8):2329–2334. doi:10.1158/1078-0432.CCR-06-1109
12. Jones SE, Erban J, Overmoyer B, et al. Randomized Phase III study of docetaxel compared with paclitaxel in metastatic breast cancer. *J Clin Oncol*. 2005;23(24):5542–5551. doi:10.1200/JCO.2005.02.027

13. Sparreboom A, Scripture CD, Trieu V, et al. Comparative preclinical and clinical pharmacokinetics of a cremophor-free, nanoparticle albumin-bound paclitaxel (ABI-007) and paclitaxel formulated in Cremophor (Taxol). *Clin Cancer Res*. 2005;11(11):4136–4143. doi:10.1158/1078-0432.CCR-04-2291
14. Untch M, Jackisch C, Schneeweiss A, et al. Nab-paclitaxel versus solvent-based paclitaxel in neoadjuvant chemotherapy for early breast cancer (GeparSepto-GBG 69): a randomised, phase 3 trial. *Lancet Oncol*. 2016;17(3):345–356. doi:10.1016/S1470-2045(15
15. Kang C, Syed YY. Atezolizumab (in Combination with Nab-Paclitaxel): a Review in Advanced Triple-Negative Breast Cancer. *Drugs*. 2020;80(6):601–607. doi:10.1007/s40265-020-01295-y
16. O'Sullivan H, Collins D, O'Reilly S. Atezolizumab and Nab-Paclitaxel in Advanced Triple-Negative Breast Cancer. *N Engl J Med*. 2019;380(10):986. doi:10.1056/NEJMc1900150
17. Schmid P, Adams S, Rugo HS, et al. Atezolizumab and Nab-Paclitaxel in Advanced Triple-Negative Breast Cancer. *N Engl J Med*. 2018;379(22):2108–2121. doi:10.1056/NEJMoa1809615
18. Gradishar WJ, Tjulandin S, Davidson N, et al. Phase III trial of nanoparticle albumin-bound paclitaxel compared with polyethylated castor oil-based paclitaxel in women with breast cancer. *J Clin Oncol*. 2005;23(31):7794–7803. doi:10.1200/JCO.2005.04.937
19. Gama CI, Tully SE, Sotogaku N, et al. Sulfation patterns of glycosaminoglycans encode molecular recognition and activity. *Nat Chem Biol*. 2006;2(9):467–473. doi:10.1038/nchembio810
20. Fried M, Duffy PE. Adherence of Plasmodium falciparum to chondroitin sulfate A in the human placenta. *Science*. 1996;272(5267):1502–1504. doi:10.1126/science.272.5267.1502
21. Salanti A, Dahlback M, Turner L, et al. Evidence for the involvement of VAR2CSA in pregnancy-associated malaria. *J Exp Med*. 2004;200(9):1197–1203. doi:10.1084/jem.20041579
22. Baston-Bust DM, Gotte M, Janni W, Krussel JS, Hess AP. Syndecan-1 knock-down in decidualized human endometrial stromal cells leads to significant changes in cytokine and angiogenic factor expression patterns. *Reprod Biol Endocrinol*. 2010;8:133. doi:10.1186/1477-7827-8-133
23. Salanti A, Clausen TM, Agerbaek MO, et al. Targeting Human Cancer by a Glycosaminoglycan Binding Malaria Protein. *Cancer Cell*. 2015;28(4):500–514. doi:10.1016/j.ccell.2015.09.003
24. Bang-Christensen SR, Pedersen RS, Pereira MA, et al. Capture and Detection of Circulating Glioma Cells Using the Recombinant VAR2CSA Malaria Protein. *Cells*. 2019;8(9):58. doi:10.3390/cells8090998
25. Agerbaek MO, Bang-Christensen SR, Yang MH, et al. The VAR2CSA malaria protein efficiently retrieves circulating tumor cells in an EpCAM-independent manner. *Nat Commun*. 2018;9. doi:10.1038/S41467-018-05793-2
26. Clausen TM, Christoffersen S, Dahlback M, et al. Structural and Functional Insight into How the Plasmodium falciparum VAR2CSA Protein Mediates Binding to Chondroitin Sulfate A in Placental Malaria. *J Biol Chem*. 2012;287(28):23332–23345. doi:10.1074/jbc.M112.348839
27. Dahlback M, Jorgensen LM, Nielsen MA, et al. The Chondroitin Sulfate A-binding Site of the VAR2CSA Protein Involves Multiple N-terminal Domains. *J Biol Chem*. 2011;286(18):15908–15917. doi:10.1074/jbc.M110.191510
28. Bordbar B, Tuikue-Ndam N, Bigey P, Doritchamou J, Scherman D, Deloron P. Identification of Id1-DBL2X of VAR2CSA as a key domain inducing highly inhibitory and cross-reactive antibodies. *Vaccine*. 2012;30(7):1343–1348. doi:10.1016/j.vaccine.2011.12.065
29. Zhang BZ, Tan LB, Yu Y, et al. Placenta-specific drug delivery by trophoblast-targeted nanoparticles in mice. *Theranostics*. 2018;8(10):2765–2781. doi:10.7150/thno.22904
30. Mitchell MJ, Billingsley MM, Haley RM, Wechsler ME, Peppas NA, Langer R. Engineering precision nanoparticles for drug delivery. *Nat Rev Drug Discov*. 2021;20(2):101–124. doi:10.1038/s41573-020-0090-8
31. Wang YF, Zhang YX, Wang JJ, Liang XJ. Aggregation-induced emission (AIE) fluorophores as imaging tools to trace the biological fate of nano-based drug delivery systems. *Adv Drug Deliver Rev*. 2019;143:161–176. doi:10.1016/j.addr.2018.12.004
32. Yuan YY, Liu B. Visualization of drug delivery processes using AIEgens. *Chem Sci*. 2017;8(4):2537–2546. doi:10.1039/c6sc05421h
33. Cao H, Yue Z, Gao H, et al. In Vivo Real-Time Imaging of Extracellular Vesicles in Liver Regeneration via Aggregation-Induced Emission Luminogens. *ACS nano*. 2019;13(3):3522–3533. doi:10.1021/acsnano.8b09776
34. Lu L, Li B, Ding S, et al. NIR-II bioluminescence for in vivo high contrast imaging and in situ ATP-mediated metastases tracing. *Nat Commun*. 2020;11(1):4192. doi:10.1038/s41467-020-18051-1
35. Xu Y, Li C, Xu R, et al. Tuning molecular aggregation to achieve highly bright AIE dots for NIR-II fluorescence imaging and NIR-I photoacoustic imaging. *Chem Sci*. 2020;11(31):8157–8166. doi:10.1039/d0sc03160g
36. Liedtke C, Mazouni C, Hess KR, et al. Response to neoadjuvant therapy and long-term survival in patients with triple-negative breast cancer. *J Clin Oncol*. 2008;26(8):1275–1281. doi:10.1200/JCO.2007.14.4147
37. Smerage JB, Barlow WE, Hortobagyi GN, et al. Circulating tumor cells and response to chemotherapy in metastatic breast cancer: SWOG S0500. *J Clin Oncol*. 2014;32(31):3483–3489. doi:10.1200/JCO.2014.56.2561
38. Hartkopf AD, Wagner P, Wallwiener D, Fehm T, Rothmund R. Changing levels of circulating tumor cells in monitoring chemotherapy response in patients with metastatic breast cancer. *Anticancer Res*. 2011;31(3):979–984.
39. Micalizzi DS, Haber DA, Maheswaran S. Cancer metastasis through the prism of epithelial-to-mesenchymal transition in circulating tumor cells. *Mol Oncol*. 2017;11(7):770–780. doi:10.1002/1878-0261.12081
40. Bidard FC, Michiels S, Riethdorf S, et al. Circulating Tumor Cells in Breast Cancer Patients Treated by Neoadjuvant Chemotherapy: a Meta-analysis. *J Natl Cancer Inst*. 2018;110(6):560–567. doi:10.1093/jnci/djy018
41. Turkman YE, Sakibia Opong A, Harris LN, Knobf MT. Biologic, demographic, and social factors affecting triple negative breast cancer outcomes. *Clin J Oncol Nurs*. 2015;19(1):62–67. doi:10.1188/15.CJON.62-67
42. Collignon J, Lousberg L, Schroeder H, Jerusalem G. Triple-negative breast cancer: treatment challenges and solutions. *Breast Cancer*. 2016;8:93–107. doi:10.2147/BCTT.S69488
43. Dawood S. Triple-negative breast cancer: epidemiology and management options. *Drugs*. 2010;70(17):2247–2258. doi:10.2165/11538150-000000000-00000
44. Ayres Pereira M, Mandel Clausen T, Pehrson C, et al. Placental Sequestration of Plasmodium falciparum Malaria Parasites Is Mediated by the Interaction Between VAR2CSA and Chondroitin Sulfate A on Syndecan-1. *PLoS Pathog*. 2016;12(8):e1005831. doi:10.1371/journal.ppat.1005831

45. Zhao K, Cheng GG, Zhang BZ, et al. Targeting delivery of partial VAR2CSA peptide guided N-2-Hydroxypropyl trimethyl ammonium chloride chitosan nanoparticles for multiple cancer types. *Mat Sci Eng C-Mater*. 2020;106:110171. doi:10.1016/J.Msec.2019.110171
46. Li WM, Mayer LD, Bally MB. Prevention of antibody-mediated elimination of ligand-targeted liposomes by using poly(ethylene glycol)-modified lipids. *J Pharmacol Exp Ther*. 2002;300(3):976–983. doi:10.1124/jpet.300.3.976
47. Garcia-Murillas I, Chopra N, Comino-Mendez I, et al. Assessment of Molecular Relapse Detection in Early-Stage Breast Cancer. *JAMA Oncol*. 2019;5(10):1473–1478. doi:10.1001/jamaoncol.2019.1838
48. Piao JG, Wang LM, Gao F, You YZ, Xiong YJ, Yang LH. Erythrocyte Membrane Is an Alternative Coating to Polyethylene Glycol for Prolonging the Circulation Lifetime of Gold Nanocages for Photothermal Therapy. *ACS nano*. 2014;8(10):10414–10425. doi:10.1021/nn503779d
49. Mocan T, Matea CT, Cojocaru I, et al. Photothermal Treatment of Human Pancreatic Cancer Using PEGylated Multi-Walled Carbon Nanotubes Induces Apoptosis by Triggering Mitochondrial Membrane Depolarization Mechanism. *J Cancer*. 2014;5(8):679–688. doi:10.7150/jca.9481
50. Hu W, Miao X, Tao H, et al. Manipulating Nonradiative Decay Channel by Intermolecular Charge Transfer for Exceptionally Improved Photothermal Conversion. *ACS nano*. 2019;13(10):12006–12014. doi:10.1021/acsnano.9b06208
51. Qi J, Sun C, Li D, et al. Aggregation-Induced Emission Luminogen with Near-Infrared-II Excitation and Near-Infrared-I Emission for Ultradeep Intravital Two-Photon Microscopy. *ACS nano*. 2018;12(8):7936–7945. doi:10.1021/acsnano.8b02452
52. Cheng Y, Bao D, Chen X, et al. Microwave-triggered/HSP-targeted gold nano-system for triple-negative breast cancer photothermal therapy. *Int J Pharm*. 2021;593:120162. doi:10.1016/j.ijpharm.2020.120162
53. Zhang J, Wang N, Li Q, Zhou Y, Luan Y. A two-pronged photodynamic nanodrug to prevent metastasis of basal-like breast cancer. *Chem commun*. 2021;57(18):2305–2308. doi:10.1039/d0cc08162k